Measurement of solid–liquid interfacial energy in the pyrene succinonitrile monotectic system

2006 J. Phys.: Condens. Matter 18 8403

(http://iopscience.iop.org/0953-8984/18/37/001)

INSTITUTE OF PHYSICS PUBLISHING JOURNAL OF PHYSICS: CONDENSED MATTER

J. Phys.: Condens. Matter **18** (2006) 8403–8412 doi:10.1088/0953-8984/18/37/001

Measurement of solid–liquid interfacial energy in the pyrene succinonitrile monotectic system

S Akbulut[1], Y Ocak[1], U Böyük[1], M Erol[1,2], K Keşlioğlu[3] and N Maraşlı[3,4]

[1] Institute of Science and Technology, Department of Physics, Erciyes University, 38039 Kayseri, Turkey
[2] Department of Physics, Faculty of Arts and Sciences, Erciyes University, 66100 Yozgat, Turkey
[3] Department of Physics, Faculty of Arts and Sciences, Erciyes University, 38039 Kayseri, Turkey

E-mail: marasli@erciyes.edu.tr

Received 7 March 2006, in final form 19 July 2006
Published 24 August 2006
Online at stacks.iop.org/JPhysCM/18/8403

Abstract

The equilibrated grain boundary groove shapes for solid pyrene (PY) in equilibrium with the PY succinonitrile (SCN) monotectic liquid were directly observed. From the observed grain boundary groove shapes, the Gibbs–Thomson coefficient and solid–liquid interfacial energy for solid PY in equilibrium with the PY SCN monotectic liquid have been determined to be $(8.72 \pm 0.87) \times 10^{-8}$ K m and $(21.9 \pm 3.28) \times 10^{-3}$ J m^{-2} with the present numerical method and Gibbs–Thomson equation, respectively. The grain boundary energy of the solid PY phase has been determined to be $(42.84 \pm 7.28) \times 10^{-3}$ J m^{-2} from the observed grain boundary groove shapes. Thermal conductivities of solid and liquid phases for PY–2.5 mol% SCN alloy and pure PY have also been measured.

1. Introduction

The solid–liquid interfacial energy, σ_{SL}, is the reversible work required to create a unit area of the interface and plays a central role in determining the nucleation rate and growth morphology of crystals. The measurement of σ_{SL} for pure materials and alloys is difficult. One of the most common techniques for determining the solid–liquid interface energy is using the equilibrated grain boundary groove shapes. In this technique, the solid–liquid interface is equilibrated with a grain boundary in a temperature gradient as shown in figure 1. The Gibbs–Thomson coefficient and solid–liquid interfacial energy are obtained using the equilibrium shape of the groove profile. This technique has been used to directly measure the solid–liquid interfacial energy for transparent materials [1–15] and for opaque materials [16–23].

[4] Author to whom any correspondence should be addressed.

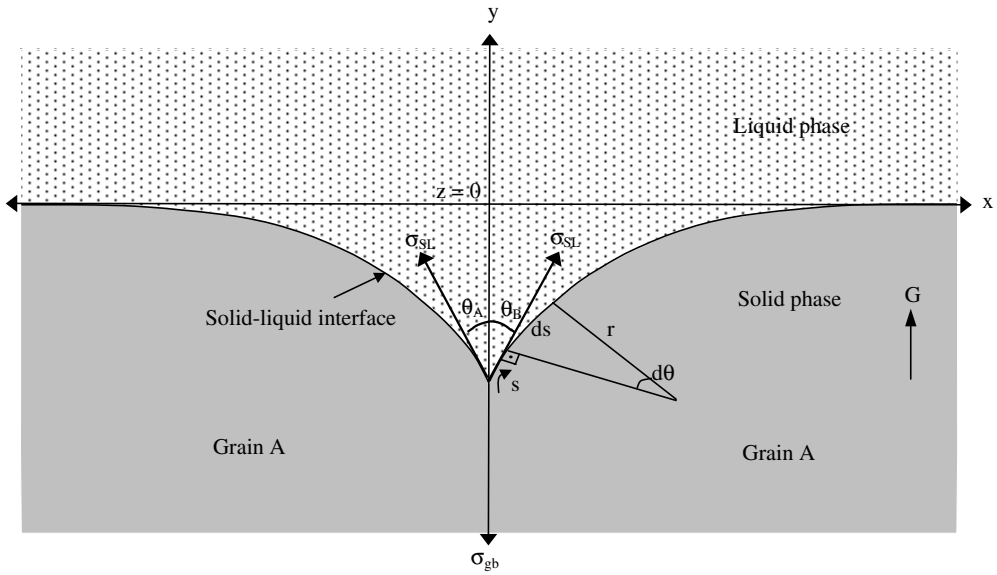

Figure 1. Schematic illustration of an equilibrated grain boundary groove formed at a solid–liquid interface in a temperature gradient showing the x, y coordinates and angle θ.

The Gibbs–Thomson coefficient, Γ, is expressed in the form of a change in undercooling, ΔT_r, with radius, r, as

$$\Delta T_r = \frac{\Gamma}{r}. \tag{1}$$

Equation (1) may be integrated in the y direction (perpendicular to the macroscopic interface) from the flat interface to a point on the cusp [16]

$$\int_0^y \Delta T_r \, \mathrm{d}y = \Gamma \int_0^y \frac{1}{r} \, \mathrm{d}y. \tag{2}$$

The right-hand side of equation (2) may be evaluated [16] for any shape by defining $\mathrm{d}s = r \, \mathrm{d}\theta$ as shown in figure 1 (s is the distance along the interface and θ is the angle that the interface makes with y) giving

$$\int_0^y \frac{1}{r} \, \mathrm{d}y = (1 - \sin\theta). \tag{3}$$

The left-hand side of equation (2) may be evaluated if ΔT_r is known as a function of y.

The left-hand side of equation (2) was integrated numerically using the values of ΔT_r calculated numerically and the right-hand side of equation (2) was evaluated by measuring the value of θ (obtained by fitting a Taylor expansion to adjacent points on the cusp) by Gündüz and Hunt [16]. This allows the Gibbs–Thomson coefficient to be determined for a measured grain boundary groove shape. This numerical method calculates the temperature along the interface of a measured grain boundary groove shape rather than attempting to predict the equilibrium grain boundary groove shape. To get accurate values of the Gibbs–Thomson coefficient with Gündüz and Hunt's numerical method, the coordinates of the grain boundary groove shape, the temperature gradient in the solid phase, G_S and the thermal conductivity ratio of the equilibrated liquid phase to the solid liquid phase, $R = K_\mathrm{L}/K_\mathrm{S}$ must be known or measured.

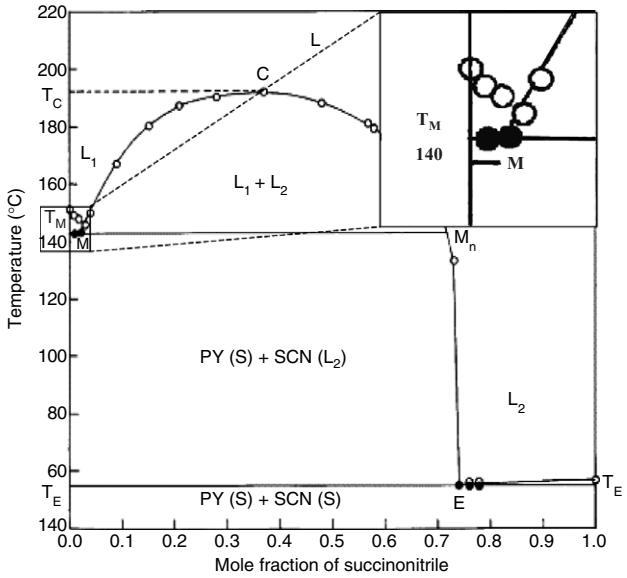

Figure 2. Phase diagram of the pyrene–succinonitrile binary system.

The solid–liquid interface energy is obtained from the thermodynamic definition of the Gibbs–Thomson coefficient, which is expressed as

$$\Gamma = \frac{\sigma_{SL}}{\Delta S^*} \tag{4}$$

where ΔS^* is the entropy of fusion per unit volume.

Recently, the phase diagram of the PY SCN system has been determined [24] and it is shown in figure 2. Although PY has a similar solidification structure to metallic materials it could not be used as an organic analogue materials because of some thermophysical properties of PY such as the solid–liquid interfacial energy, Gibbs–Thomson coefficient and thermal conductivity have not been determined or known. No attempts were made to determine the solid–liquid interfacial energy and Gibbs–Thomson coefficient for PY due to its higher melting temperature (424.15 K). Thus the goal of the present work is to determine the thermal conductivity for the solid and liquid phases, Gibbs–Thomson coefficient, solid–liquid interfacial energy and grain boundary energy for solid PY in equilibrium with the PY SCN monotectic liquid.

2. Experimental details

2.1. Sample production

The equilibrated solid PY in equilibrium with the PY SCN monotectic liquid has been directly observed using a temperature gradient stage. The details of the apparatus and experimental procedures are given in [9–11]. The specimen cell was made by sticking two glass cover slips (50 mm long, 24 mm wide and 0.15 mm thick) with silicone elastomer glue. The slides were placed with their largest surface in the x–y plane and spaced a distance of about 80–100 μm apart in the z direction to minimize heat flow and curvature in the z direction and observe the equilibrated grain boundary groove shapes in the x–y plane (2D). Organic materials usually react with this type of glue, so before filling the cell with alloy, the cell was annealed at 523 K to prevent any reaction with glue.

Consider a binary monotectic system as shown in figure 2. Above the monotectic temperature, a binary monotectic system consists of liquid provided that the alloy composition $C_0 < C_\alpha$, where C_α is the composition of the monotectic solid α. If the system is held in a very stable temperature gradient, the liquid droplets move to the hotter parts by temperature gradient zone melting (TGZM) and a single solid phase (solid α) in equilibrium with the monotectic liquid can grow on the monotectic structure during the annealing period.

The phase diagram of the PY SCN monotectic system is shown in figure 2. In the present work, the alloy composition was chosen to be PY–1 mol% SCN to observe a single solid PY in equilibrium with the monotectic liquid (PY–2.5 mol% SCN). PY–1 mol% SCN alloy was prepared from the >99% purity PY and 99% purity SCN supplied by Sigma-Aldrich Chemical Company. No attempt was made to purify the compounds. Known masses of PY and SCN were placed in a glass flask. The glass flask was then tightly sealed and melted in the furnace. Thus an alloy was formed by the mixing of the components.

2.2. The temperature gradient measurement

After the specimen cell was filled with organic alloy, the specimen was placed in a temperature gradient stage. A temperature gradient was established on the specimen by using heaters of two different types; one of them was an electrical heater and the other was a circulating bath. One side of the specimen was melted with the electrical heater and the other side was kept cool with the circulating bath. The temperature of the electrical heater was controlled to an accuracy ± 0.01 K with a *Eurotherm 2604* type of controller and the temperature of the circulating bath was kept constant (343 K) to an accuracy ± 0.01 K with a *PolyScience Digital 9102 Model Heating/Refrigerating Circulating Bath*. The temperatures in the specimen were measured using three insulated K-type thermocouples with wires 50 μm thick. The ends of the thermocouple wires were spark-welded. Thermocouples were placed at a distance of about 1–2 mm from each other and perpendicular to the heat flow direction in the specimen. The thermocouples were calibrated by detecting the monotectic melting point of the PY–2.5 mol% SCN alloy. The melting point of the PY–2.5 mol% SCN alloy was measured with an accuracy of ± 0.3 K. The specimen was melted until two of the three thermocouples were in the liquid phase and left to reach equilibrium. Then planar growth was begun with a very low growth rate (8.3×10^{-4} cm s^{-1}). The temperature of the planar interface was measured with two thermocouples. The difference between two thermocouple readings was ± 0.2 K.

A thin liquid layer (2 or 3 mm thick) was melted to produce uniform monotectic liquid and the specimen was held in a constant temperature gradient to observe a single solid PY in equilibrium with the monotectic liquid. The equilibrating time was one day for the PY–1 mol% SCN alloy. When the solid–liquid interface reached equilibrium, the temperature difference between two thermocouples, ΔT, was measured using a Hewlett-Packard 34401A model digital multimeter. The multimeter has a 1 μV resolution for direct voltage measurements. The positions of the thermocouples and the equilibrated grain boundary groove shapes were then photographed with a CCD digital camera placed in conjunction with an Olympus BH2 light optical microscope. The distance between two thermocouples, ΔX, was measured using Adobe PhotoShop 7.0 version software from the photographs of the thermocouple positions.

The temperature gradient, $G = \Delta T/\Delta X$, for the equilibrated grain boundary groove shapes was determined using the values of ΔT and ΔX. The estimated error in the measurements of the temperature gradient, G, is about 5% [11].

The coordinates of the equilibrated grain boundary groove shapes were measured with an optical microscope to an accuracy of ± 10 μm. The uncertainty in the measurements of equilibrated grain boundary coordinates was 0.1%.

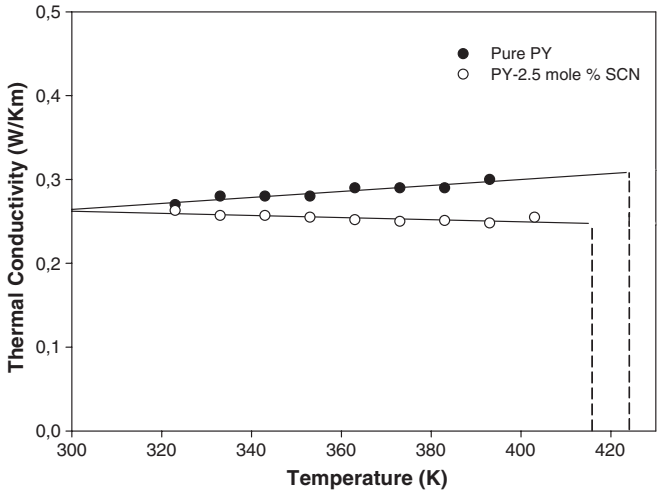

Figure 3. Thermal conductivities of solid phase versus time for pure PY and PY–2.5 mol% SCN alloys.

2.3. Thermal conductivity ratio of liquid phase to solid phase

The thermal conductivity ratio of the monotectic liquid phase to solid PY phase, $R = K_{\mathrm{L\,(monotectic\,liquid)}}/K_{\mathrm{S\,(solid\,PY)}}$, must be known or measured to evaluate the Gibbs–Thomson coefficients with the present numerical method. The radial heat flow method is an ideal technique for measuring the conductivities in the solid. The thermal conductivities of the monotectic solid phase and solid pure PY phase are needed to evaluate the value of $R = K_{\mathrm{L\,(monotectic\,liquid)}}/K_{\mathrm{S\,(solid\,PY)}}$. In the radial heat flow method, a cylindrical sample was heated by using a single heating wire along the axis at the centre of the sample and the sample was kept in a very stable temperature gradient for a period to achieve the steady state condition. At the steady state condition, the temperature gradient in the cylindrical specimen is given by Fourier's law

$$\frac{\mathrm{d}T}{\mathrm{d}r} = -\frac{Q}{AK_{\mathrm{S}}} \tag{5}$$

where Q is the total input power from the centre of the specimen, A is the surface area of the specimen and K_{S} is the thermal conductivity of the solid phase. Integration of the equation (5) gives

$$K_{\mathrm{S}} = \frac{1}{2\pi\ell}\ln\left(\frac{r_2}{r_1}\right)\frac{Q}{T_1 - T_2} \tag{6}$$

$$K_{\mathrm{S}} = a_0\frac{Q}{T_1 - T_2} \tag{7}$$

where $a_0 = \ln(r_2/r_1)/2\pi\ell$ is an experimental constant, r_1 and r_2 ($r_2 > r_1$) are fixed distances from the centre axis of the specimen, ℓ is the length of the heating wire which is constant and T_1 and T_2 are the temperatures at the fixed positions, r_1 and r_2, from the centre axis of the specimen. Equation (7) could be used to obtain the conductivity of the solid phase by measuring the difference in temperature between the two fixed points for a given power level.

The thermal conductivities of monotectic solid phase and solid PY were measured with a radial heat flow apparatus. The details of the radial heat flow apparatus and technique are given in [16, 20, 25]. The sample was heated using the central heating wire in steps of 10 K up to 5 K

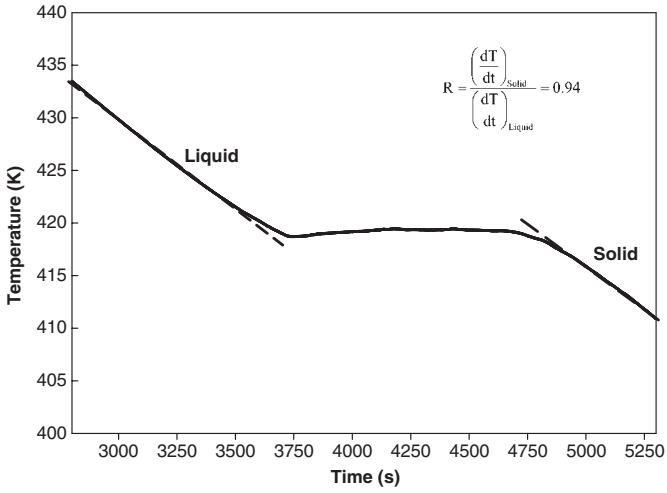

Figure 4. Temperature versus time for the PY–2.5 mol% SCN alloy.

Table 1. The thermal conductivities of solid and liquid phases and their ratios at their melting temperature for pure PY and the PY SCN binary monotectic system.

System	Phases	Temperature (K)	K (W K^{-1} m^{-1})	$R = K_L/K_S$
Pure PY	Liquid PY	424.15	0.242	0.89
	Solid PY		0.272	
Monotectic PY SCN	Liquid (PY–2.5 mol% SCN)	416.45	0.235	0.94
	Solid (PY–2.5 mol% SCN)		0.250	
	Liquid (PY–2.5 mol% SCN)		0.235	0.86
	Solid PY		0.272	

below the monotectic melting temperature. The samples were kept at steady state for at least 2 h. At steady state the total input power and the temperatures were measured. When all desired power and temperature measurements had been completed the sample was left to cool to room temperature. The thermal conductivities of the monotectic solid phase and solid pure PY versus temperature are shown in figure 3. The values of the thermal conductivity of $K_{S\,(\text{monotectic solid})}$ and $K_{S\,(\text{solid PY})}$ at their melting temperatures were obtained as 0.250 and 0.272 W K^{-1} m^{-1} by extrapolating to the melting temperatures, respectively.

It is not possible to measure the thermal conductivity of the liquid phase with the radial heat flow apparatus since a thick liquid layer (10 mm) is required. A layer of this size would certainly have led to convection. If the ratio of thermal conductivity of the liquid phase to solid phase is known and the thermal conductivity of the solid phase is measured at the monotectic (or melting) temperature, the thermal conductivity of the liquid phase can then be evaluated. The thermal conductivity ratio of monotectic liquid phase to monotectic solid phase was measured in a directional growth apparatus. A thin vertical glass tube, 5 mm OD and 3 mm ID, was used to minimize convection in the liquid phase. The time–temperature traces enable the conductivity ratio of the liquid phase to solid phase to be calculated [16–18]. The thermal conductivity ratio of monotectic liquid phase to solid phase was found to be 0.94 from the time–temperature trace which is given in figure 4. Thus the thermal conductivity of the monotectic liquid phase, $K_{L\,(\text{monotectic liquid})}$, is obtained as 0.235 W K^{-1} m^{-1}. The measured values of thermal conductivities for the PY SCN monotectic system are given in table 1. The value of

Table 2. Gibbs–Thomson coefficients for solid PY in equilibrium with PY SCN monotectic liquid. The subscripts LHS and RHS refer to left-hand side and right-hand side of groove, respectively. ($\bar{\Gamma} = (8.72 \pm 0.87) \times 10^{-8}$ K m for solid PY in equilibrium with PY SCN monotectic liquid.)

Groove no.	$G_S \times 10^2$ (K m^{-1})	Gibbs–Thomson coefficient Γ (K m)	
		$\Gamma_{LHS} \times 10^{-8}$	$\Gamma_{RHS} \times 10^{-8}$
a	47.54	8.68	8.66
b	50.34	8.73	8.65
c	49.94	8.70	8.72
d	47.19	8.70	8.70
e	47.77	8.70	8.75
f	47.07	8.75	8.80
g	50.29	8.75	8.63
h	48.63	8.72	8.77
i	46.14	8.70	8.78
j	48.58	8.72	8.75

$R = K_{L\,(\text{monotectic liquid})}/K_{S\,(\text{solid PY})}$ was found to be 0.86 and it is also given in table 1. The estimated error in the measurements of the thermal conductivity of the solid and liquid phase was about 5% [25].

3. Results and discussion

3.1. The Gibbs–Thomson coefficient

If the thermal conductivity ratio of the equilibrated liquid phase to solid phase, $R = K_L/K_S$, the coordinates of the grain boundary groove shapes and the temperature gradient in the solid phase G are known, then the Gibbs–Thomson coefficient can be obtained using the numerical method described in detail in [16]. The experimental error in the determination of Gibbs–Thomson coefficient is the sum of experimental errors of the measurements of the temperature gradient and thermal conductivity. Thus the total error in the determination of Gibbs–Thomson coefficient was about 10%.

The Gibbs–Thomson coefficients for solid PY in equilibrium with the PY SCN monotectic liquid were determined by the numerical method using ten observed grain boundary groove shapes and the results are given in table 2. Typical grain boundary groove shapes for solid PY in equilibrium with the PY SCN monotectic liquid examined in the present work are shown in figure 5.

The average value of Γ with experimental error from table 2 is $(8.72 \pm 0.87) \times 10^{-8}$ K m for solid PY in equilibrium with the PY SCN monotectic liquid.

3.2. The entropy of fusion per unit volume

To determine the solid–liquid interface energy it is also necessary to know the entropy of fusion per unit volume and this is given by

$$\Delta S^* = \frac{\Delta H_M}{T_M}\frac{1}{V_S} \tag{8}$$

where ΔH_M is the enthalpy of primary solid phase in the binary monotectic system at the melting temperature, T_M is the melting temperature and V_S is the molar volume of primary phase. The values of T_M, V_S and ΔS^* are given in table 3. The error in the determination of the entropy of fusion per unit volume is estimated to be about 5% [16, 26].

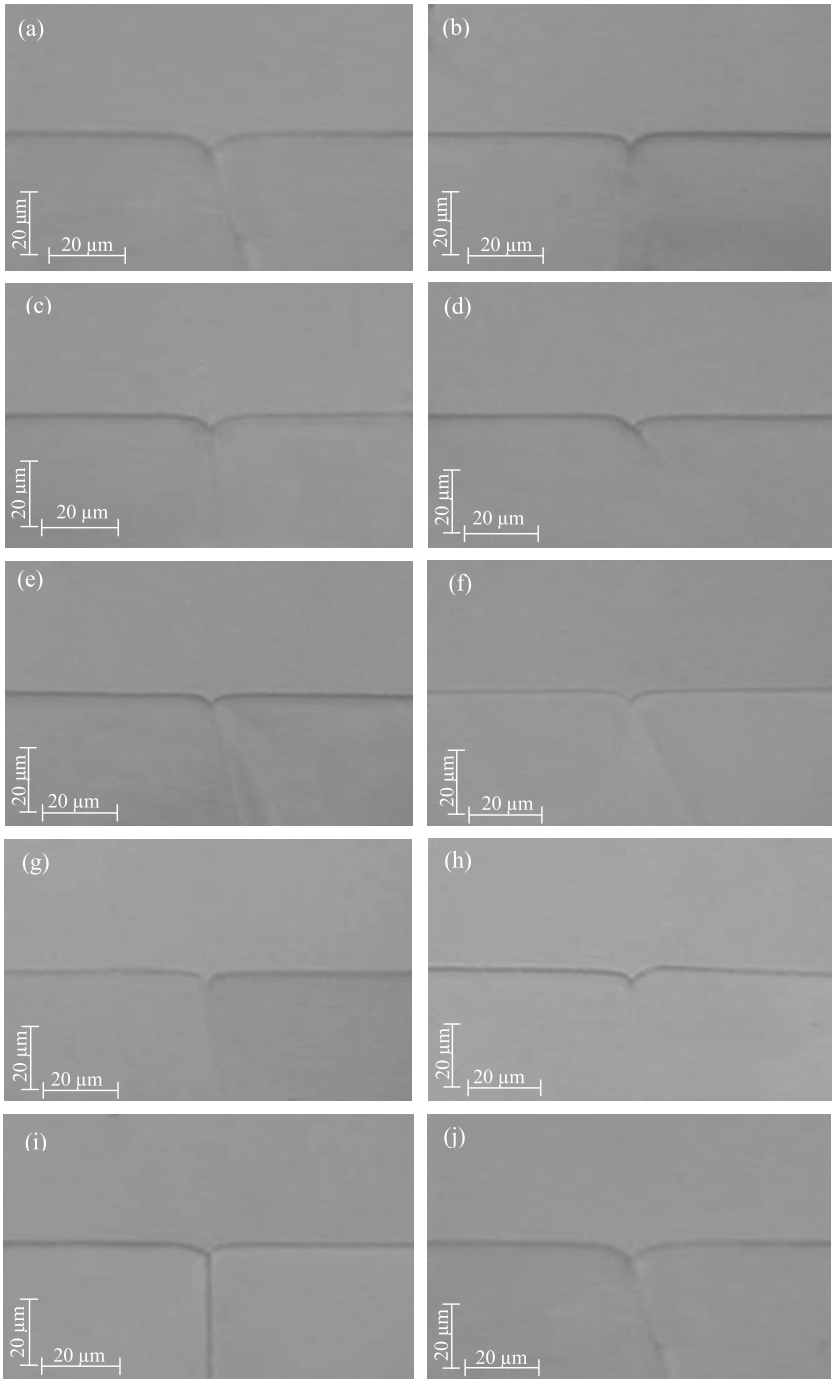

Figure 5. Typical grain boundary groove shapes for solid PY in equilibrium with the PY SCN monotectic liquid.

Table 3. Some physical properties of PY SCN monotectic system.

System	PY SCN
Solid phase (C_S)	PY
Liquid phase (C_L)	PY–2.5 mol% SCN
$T_{monotectic}$	416.45 (K) [24]
m (molecular weight of PY)	202.26×10^{-3} (kg mol^{-1})
d (density of PY)	1.271×10^{3} (kg m^{-3})
V_S (molecular volume of PY)	159.13×10^{-6} (m^3 mol^{-1})
ΔH_M	16.6×10^{3} (J mol^{-1}) [24]
ΔS^*	2.51×10^{5} (J K^{-1} m^{-3})

Table 4. A comparison of the calculated values of σ_{SL} with the experimental values of σ_{SL} for some organic materials.

Organic materials	ΔH (J mol^{-1})	$V_S \times 10^{-6}$ (m^3 mol^{-1})	Solid–liquid interface energy, $\sigma_{SL} \times 10^{-3}$ (J m^{-2})	
			Calculated with equation (9)	Experimental
Succinonitrile	3 484 [28]	76.5	7.78	7.86 [11]
(D) camphor	6 865 [28]	153.8	9.63	10.75 [15]
Pivalic acid	2 427 [8]	112.7	4.18	2.67 [9], 2.84 [8]
Camphene	2 706 [29]	161.8	3.67	4.42 [10]
Pyrene	16 600 [24]	159.13	22.76	21.89 [present work]

3.3. The solid–liquid interface energy

If the values of the Gibbs–Thomson coefficient and the entropy of fusion per unit volume are measured or known, the solid–liquid interface energy can be obtained from equation (4). The experimental error in the determined solid–liquid interface energy is the sum of experimental errors of Gibbs–Thomson coefficient and entropy of fusion per unit volume. Thus the total experimental error in the determination of the solid–liquid interface energy with the present method was about 15%. The value of the solid–liquid interfacial energy, σ_{SL}, for solid PY in equilibrium with the PY SCN monotectic liquid was found to be $(21.90 \pm 3.28) \times 10^{-3}$ J m^{-2}.

On the basis of nucleation experiments and classical nucleation theory, Turnbull [27] proposed an empirical relationship between the interfacial energy and melting enthalpy change for estimating the interfacial energy and it is expressed as [27]

$$\sigma_{SL} = \frac{\tau \Delta H_m}{V_S^{2/3} N_a^{1/3}} \tag{9}$$

where the coefficient τ was found to be 0.45 for metals and 0.34 for nonmetallic systems [27] and N_a is the Avogadro constant. Comparisons of the calculated values of σ_{SL} from equation (9) with the experimental values of σ_{SL} for different organic materials are given in table 4. As can be seen from table 4, the calculated values of σ_{SL} are in good agreement with the experimental values of σ_{SL} except for pivalic acid.

3.4. The grain boundary energy

The grain boundary energy can be expressed as

$$\sigma_{gb} = 2\sigma_{SL} \cos\theta \tag{10}$$

where $\theta = \frac{\theta_A + \theta_B}{2}$ is the angle that the solid–liquid interfaces make with the y axis [11, 30]. The angles, θ_A and θ_B, were obtained from the cusp coordinates, x, y, using a Taylor expansion

for parts at the base of the groove. The grain boundary energy was then calculated from equation (10) using the solid–liquid interface energy and the values of θ. The estimated error in determination of the angles was found to be 2% from the standard deviation. Thus the total experimental error in the resulting grain boundary energy is about 17%. The value of σ_{gb} for solid PY was found to be $(42.84 \pm 7.28) \times 10^{-3}$ J m^{-2}.

4. Conclusions

The equilibrated grain boundary groove shapes for solid PY in equilibrium with the PY SCN monotectic liquid were directly observed in a constant temperature gradient. From the observed grain boundary groove shapes, the Gibbs–Thomson coefficient, solid–liquid interface energy and the grain boundary energy for solid PY in equilibrium with the PY SCN monotectic liquid have been determined. Thermal conductivities of solid and liquid phases for PY–2.5 mol% SCN and pure PY alloy have also been measured.

Acknowledgments

This project was supported by Erciyes University Scientific Research Project Unit under Contract No. FBT-06-38. The authors would like to thank Erciyes University Research Foundation for financial support.

References

[1] Jones D R H and Chadwick G A 1970 *Phil. Mag.* **22** 291
[2] Jones D R H and Chadwick G A 1971 *J. Cryst. Growth* **11** 260
[3] Jones D R H 1978 *Phil. Mag.* **27** 569
[4] Schaefer R J, Glicksman M E and Ayers J D 1975 *Phil. Mag.* **32** 725
[5] Hardy S C 1977 *Phil. Mag.* **35** 471
[6] Nash G E and Glicksman M E 1971 *Phil. Mag.* **24** 577
[7] Bolling G F and Tiller W A 1960 *J. Appl. Phys.* **31** 1345
[8] Singh N B and Glicksman M E 1989 *J. Cryst. Growth* **98** 573
[9] Bayender B, Maraşlı N, Çadırlı E, Şişman H and Gündüz M 1998 *J. Cryst. Growth* **194** 119
[10] Bayender B, Maraşlı N, Çadırlı E and Gündüz M 1999 *Mater. Sci. Eng.* A **270** 343
[11] Maraşlı N, Keşlioğlu K and Arslan B 2003 *J. Cryst. Growth* **247** 613
[12] Stalder I and Bilgram J H 2003 *J. Chem. Phys.* **118** 798
[13] Böyük U, Keşlioğlu K, Erol M and Maraşlı N 2005 *Mater. Lett.* **59** 2953
[14] Keşlioğlu K, Böyük U, Erol M and Maraşlı N 2006 *J. Mater. Sci.* at press
[15] Ocak Y, Akbulut S, Böyük U, Erol M, Keşlioğlu K and Maraşlı N 2006 *Scr. Mater.* **55** 235
[16] Gündüz M and Hunt J D 1985 *Acta Metall.* **33** 1651
[17] Gündüz M and Hunt J D 1989 *Acta Metall.* **37** 1839
[18] Maraşlı N and Hunt J D 1996 *Acta Mater.* **44** 1085
[19] Keşlioğlu K and Maraşlı N 2004 *Mater. Sci. Eng.* A **369** 294
[20] Keşlioğlu K and Maraşlı N 2004 *Metall. Mater. Trans.* A **35A** 3665
[21] Keşlioğlu K, Gündüz M, Kaya H and Çadırlı E 2004 *Mater. Lett.* **58** 3067
[22] Erol M, Maraşlı N, Keşlioğlu K and Gündüz M 2004 *Scr. Mater.* **51** 131
[23] Keşlioğlu K, Erol M, Maraşlı N and Gündüz M 2004 *J. Alloys Compounds* **385** 207
[24] Rai U S and Pink P 2003 *J. Cryst. Growth* **249** 301
[25] Erol M, Keşlioğlu K, Şahingöz R and Maraşlı N 2005 *Met. Mater. Int.* **11** 421
[26] Tassa M and Hunt J D 1976 *J. Cryst. Growth* **34** 38
[27] Turnbull D 1950 *J. Appl. Phys.* **21** 1022
[28] Witusiewicz V T, Sturz L, Hecht U and Rex S 2004 *Acta Mater.* **52** 4561
[29] Rubinstein E R and Glicksman M E 1991 *J. Cryst. Growth* **112** 97
[30] Woodruff P 1973 *The Solid–Liquid Interface* (Cambridge: Cambridge University Press)